catalysts

MDPI

Article

Photocatalytic H_2 Production from Naphthalene by Various TiO_2 Photocatalysts: Impact of Pt Loading and Formation of Intermediates

Osama Al-Madanat [1,2,*], Yamen AlSalka [1,3], Ralf Dillert [1,3] and Detlef W. Bahnemann [1,3,4,*]

[1] Institut für Technische Chemie, Gottfried Wilhelm Leibniz Universität Hannover, Callinstr. 3, D-30167 Hannover, Germany; alsalka@iftc.uni-hannover.de (Y.A.); dillert@iftc.uni-hannover.de (R.D.)
[2] Chemistry Department, Mutah University, Mutah, Al-Karak 61710, Jordan
[3] Laboratorium für Nano- und Quantenengineering, Gottfried Wilhelm Leibniz Universität Hannover, Schneiderberg 39, D-30167 Hannover, Germany
[4] Laboratory "Photoactive Nanocomposite Materials", Saint-Petersburg State University, Ulyanovskaya str. 1, Peterhof, 198504 Saint-Petersburg, Russia
* Correspondence: al-madanat@iftc.uni-hannover.de (O.A.-M.); bahnemann@iftc.uni-hannover.de (D.W.B.); Tel.: +49-511-762-2773 (O.A.-M.); Fax: +49-511-762-3004 (O.A.-M.)

Abstract: This work presents a comparative study of the efficiency of two commercial TiO_2 photocatalysts, Aeroxide P25 ($ATiO_2$) and Sachtleben Hombikat UV100 ($HTiO_2$), in H_2 production from an aqueous solution of naphthalene. The TiO_2 photocatalysts were platinized by the photodeposition method varying the platinum content of the suspension to 0.5, 1.0, and 5.0 wt%. A full physicochemical characterization for these materials was performed, showing no structural effects from the deposition method, and confirming a well dispersion of nanosized-Pt^0 particles on the surface of both photocatalysts. Pristine $ATiO_2$ shows around 14% higher photocatalytic fractional conversion of naphthalene than pristine $HTiO_2$ after 240 min of irradiation, while both materials exhibit negligible activity for H_2 formation. The 0.5 wt% Pt- $HTiO_2$ increases the photocatalytic fractional conversion of naphthalene from 71% to 82% and produces 6 µmol of H_2. However, using a higher Pt content than the optimal platinization ratio of 0.5 wt% dramatically inhibits both processes. On the other hand, regardless of the fractional ratio of Pt, the platinization of $ATiO_2$ results in a decrease in the fractional conversion of naphthalene by 4% to 33% of the pristine value. Although the presence of Pt islands on the surface of the $ATiO_2$ is essential for the H_2 evolution, no dependency between the Pt ratio and the H_2 formation rate was observed since all the platinized materials show a similar H_2 formation of around 3 µmol. Based on the EPR results, the higher photocatalytic activity of the Pt-$HTiO_2$ is attributed to the efficient charge carrier separation and its larger surface area. The recyclability test confirms that the inhibition of the photocatalytic process is related to the deactivation of the photocatalyst surface by the adsorption of the photoformed intermediates. A strong relationship between the photocatalytic activity and the kind of the aromatic compounds was observed. The H_2 evolution and the photooxidation of the aromatic hydrocarbons exhibit higher photonic efficiencies than that of their corresponding hydroxylated compounds over the Pt-$HTiO_2$.

Keywords: naphthalene; photoreforming; Hombikat UV100; Aeroxide P25; H_2 production; EPR; charge carrier; Pt-TiO_2

Citation: Al-Madanat, O.; AlSalka, Y.; Dillert, R.; Bahnemann, D.W. Photocatalytic H_2 Production from Naphthalene by Various TiO_2 Photocatalysts: Impact of Pt Loading and Formation of Intermediates. *Catalysts* **2021**, *11*, 107. https://doi.org/10.3390/catal11010107

Received: 30 November 2020
Accepted: 10 January 2021
Published: 13 January 2021

1. Introduction

Achieving a fully sustainable energy system for the future involves the development of multiple and diverse technologies. One of these systems is the renewable energy carriers, such as molecular hydrogen (H_2), which possesses advantageous properties compared to petroleum and other fossil-derived fuels [1]. It has the highest gravimetric heating density among all fuels, i.e., a heating value (HHV) of 142 MJ kg^{-1} [2], and it burns cleanly producing pure water [3]. The development of new, clean, and efficient technologies for

H_2 production from renewable resources has gained increasing attention. Undoubtedly, efficient large-scale H_2 production from industrial wastewaters containing organic matter can contribute to the implementation of an H_2 economy [4,5]

Industrial effluents are often rich in persistent organic pollutants, such as polycyclic aromatic hydrocarbons (PAHs). PAHs originate chiefly from anthropogenic processes, especially from incomplete combustion of fossil fuels and from accidental spillages of crude oil and refined fuels. The U.S. Environmental Protection Agency (EPA) classified PAHs as priority pollutants, due to their known human toxicity potential and their ubiquitous occurrence in the environment [6,7]. Among other PAHs, naphthalene is the most widespread PAH in the effluent streams of the petroleum and coal industries, which is definitely related to its relative higher water solubility in comparison to other PAHs [8]. Over the years, processes have been developed for the removal of PAHs from contaminated waters including the ultrasonic process [9], adsorption [7], biodegradation [10], pulse radiolysis [11], and heterogeneous photocatalysis [7]. To date, TiO_2 has proven its efficacy in the photocatalytic oxidation of various PAHs and especially in the remediation of naphthalene [12].

However, the development of methods for the conversion of these pollutants into chemical energy in the form of molecular hydrogen is a more attractive solution. In particular, solar photocatalysis is regarded as a promising and eco-friendly strategy for PAHs environmental remediation [7]. Solar photocatalytic reforming of organic pollutants contained in wastewaters under anaerobic conditions may be a viable alternative to other renewable hydrogen technologies. Hydrogen production from wastewater is a rapidly growing field combining water decontamination and transformation of the chemical energy stored in pollutants to molecular hydrogen and carbon dioxide. Although photocatalytic aerobic oxidation has already proven to be an effective process for the naphthalene removal from aqueous solutions [7,12,13], to our knowledge, very limited studies have been performed to investigate the photocatalytic oxidation of naphthalene under anaerobic conditions [14].

Heterogeneous photocatalysis, particularly TiO_2-based photocatalysis stands out amongst the most encouraging impetuses due to its high photo-reactivity, high photostability, low cost, and non-toxicity [15,16]. However, the major drawbacks of TiO_2 are the inability of visible light absorption and the fast recombination of photoexcited *electron/hole* (e^-/h^+) pair [17]. Aromatic hydrocarbon compounds have been rarely used in photocatalysis as sacrificial agents to enhance the H_2 production from the water splitting in the absence of O_2 [4,14,18,19]. Nevertheless, the consumption of the photo-generated holes by these agents results in the accumulation of photo-generated electrons on the TiO_2 surface. Loading the surface of TiO_2 with noble metals, in particular, platinum (Pt) nanoparticles, plays an essential role in enhancing the photocatalytic conversion process [4,20]. Interestingly, Pt nanoparticles on the surface of TiO_2 act as electron acceptors for the accumulated electrons, enhancing the formation of molecular hydrogen by reducing the overpotential of proton reduction [4,21,22].

In our previous study [14], the mechanistic pathways of the photoreforming of naphthalene on anatase TiO_2 were in-depth investigated by a novel feasible approach. However, in this study, we studied the effect of different parameters on the H_2 production by reforming of naphthalene in an aqueous medium under simulated solar light. Two different commercial TiO_2, Aeroxide P25 and Hombikat UV 100 have been used. These TiO_2 photocatalysts were platinized using a photodeposition method by varying the platinum content of the suspension. The difference in their activities was evaluated through the study of the charge carrier separation, H_2 production, and naphthalene conversion during the photocatalytic process. Moreover, the effect of the intermediate products during the photocatalytic process was also investigated.

2. Results and Discussion

2.1. Photocatalysts Characterization

The ICP-OES measurements in Table 1 show the actual content of Pt in TiO_2 samples. The results indicate an actual Pt content of all samples being approximately 10% lower than the nominal value. However, the values for each set of Pt percentage (0.50, 1.0, and 5.0 wt%) are nearly the same for different types of catalysts, and within the experimental error.

Table 1. Actual loaded Pt nanoparticles percentage, BET surface area, and crystallite size for the pristine and as-prepared platinized TiO_2.

Photocatalyst	Measured Pt wt%	BET Surface Area g m^{-2}	Crystallite Size [a] nm
$HTiO_2$ (UV100)	-	295 ± 3	8.0 ± 0.7
0.5 wt% Pt-$HTiO_2$	0.46 ± 0.02	290 ± 2	8.4 ± 1.1
1.0 wt% Pt-$HTiO_2$	0.88 ± 0.03	287 ± 2	8.9 ± 2.8
5.0 wt% Pt-$HTiO_2$	4.75 ± 0.07	278 ± 2	9.2 ± 2.1
$ATiO_2$ (P25)	-	52.3 ± 0.8	17.5 ± 6.3
0.5 wt% Pt-$ATiO_2$	0.45± 0.05	50.0 ± 0.2	18.5 ± 4.7
1.0 wt% Pt-$ATiO_2$	0.90 ± 0.05	48.0 ± 0.3	19.3 ± 5.5
5.0 wt% Pt-$ATiO_2$	4.50 ± 0.10	43.8 ± 1.2	20.6 ± 6.1

[a] The values are calculated based on the Scherrer equation.

The specific surface area (BET) values in Table 1 indicate that the pristine $HTiO_2$ possesses a larger specific surface area of 300 m^2 g^{-1}, compared to 52 m^2 g^{-1} for the pristine $ATiO_2$, which is in good agreement with previous literature reports [23,24]. Apparently, the loading of platinum on the surface of both pristine photocatalysts slightly decreases the surface area by 5.0–10%, which is consistent with the low loading amounts of platinum on the TiO_2 surface.

Figure 1 shows the XRD profiles of the pristine and platinized $HTiO_2$ and $ATiO_2$, respectively. The diffraction patterns and peak positions of the modified and unmodified $ATiO_2$ (Figure 1a) possess well-defined characteristic peaks corresponding to a mixture of anatase-rutile phases (JCPDS card No. 21-1272 and 21-1276, respectively). The intensity ratio between 101 (anatase) and 110 (rutile) main diffraction peaks is around 84:16, respectively. On the other hand, Figure 1b shows that pristine and platinized $HTiO_2$ samples fit pretty well with the XRD patterns of pure anatase TiO_2, which is in good agreement with JCPDS card No. 21-1272. The broadness of the $HTiO_2$ diffraction pattern peaks indicates less crystallinity and smaller average crystallite sizes (Table 1), which is in agreement with the high observed specific surface areas for the TiO_2 [24,25]. Mean crystallite sizes were calculated from the main diffraction peaks based on the Scherrer equation [26].

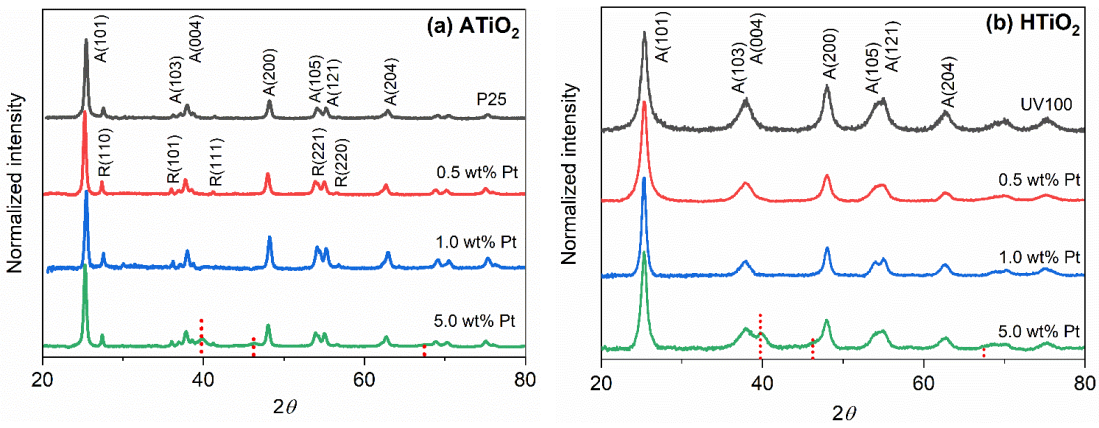

Figure 1. XRD patterns of pristine and different percentage of Pt loaded on (**a**) $ATiO_2$ and (**b**) $HTiO_2$ surfaces. A and R stand for anatase and rutile phases, respectively. The red lines in the bottom represent the Pt reference.

As revealed from Figure 1 and Table 1, the loading of Pt nanoparticles does not significantly change the XRD pattern position or features for all Pt-TiO_2 samples, indicating that the preparation method did not significantly change the phase content and the crystallinity of the TiO_2. Notably, the deposition of Pt did not generate any typical Pt diffraction peaks, which might result from the uniform distribution and the low loading amount of Pt [27]. However, in the 5.0 wt% Pt-loaded samples, two weak and broad peaks around 39.8° and 46.2° corresponding to 111 and 200 fcc platinum metal, respectively, have been observed.

The DR UV–vis spectra of pristine and platinized $ATiO_2$ and $HTiO_2$ samples were converted to their corresponding Tauc plots and shown in Figure 2. All the tested powders exhibit a similar optical bandgap of ~3.0 eV for $ATiO_2$ anatase-rutile polymorph (Figure 2a) and ~3.2 eV for the $ATiO_2$ anatase polymorph (Figure 2b) [28]. The absorption spectra for Pt-TiO_2 samples indicate that the photodeposition method does not induce a substantial variation of the bandgap energy, however, a slight shift to the visible light region has been observed, due to the color change and high absorption of platinum clusters in the visible region [29]. This optical characteristic of Pt-TiO_2 indicated that Pt nanoparticles do not exhibit localized surface plasmon absorption in the visible region, which can be attributed to a damping effect caused by d–d interband transitions [27].

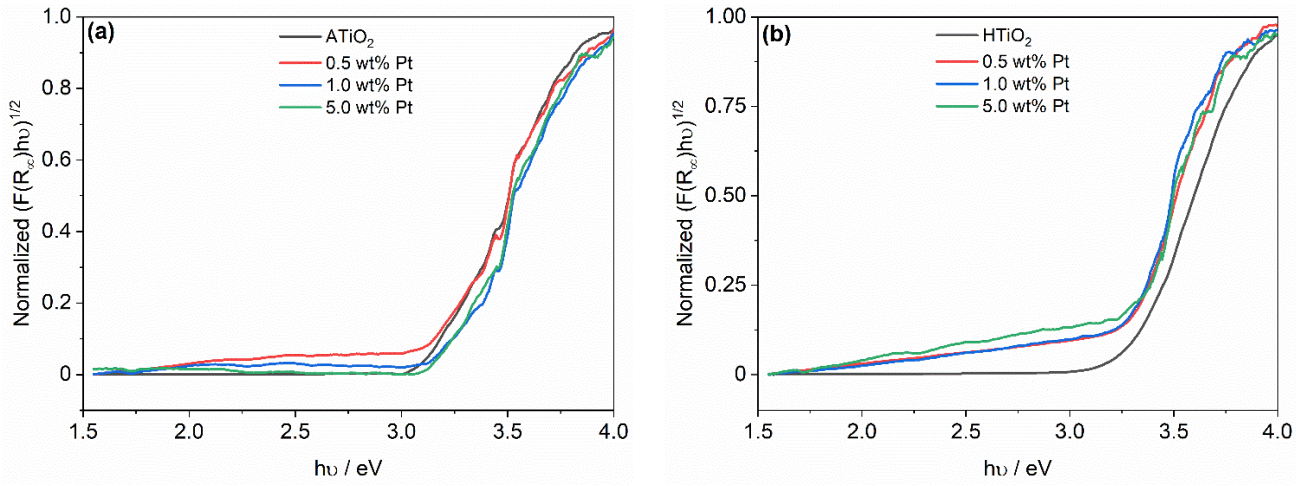

Figure 2. Normalized diffuse reflectance spectra (Tauc plot vs. photon energy) of pristine and platinized samples for (**a**) $ATiO_2$ and (**b**) $HTiO_2$.

The morphologies of the synthesized samples were investigated by high resolution-transmission electron microscopy (HRTEM). The micrographs of Figure 3 show the morphology of $ATiO_2$ and $HTiO_2$ photocatalysts before and after loading the Pt nanoparticles using the photodeposition method. The noticeable difference between the morphologies of $ATiO_2$ (Figure 3a) and $HTiO_2$ (Figure 3d) is related to the difference in their phase contents. $HTiO_2$ is a pure anatase, while $ATiO_2$ contains also a rutile phase that possesses a larger crystallite size, altering the agglomeration abilities. As shown in Figure 3a–c,d–f, the loading of Pt nanoparticles does not have any significant effect on the particle size or shape of both materials. Pt-$HTiO_2$ shows highly agglomerated small sub-particles, producing a higher specific surface area compared to Pt-$ATiO_2$. The nanoscale TiO_2 samples show sizes with different diameters of about 20–25 nm for Pt-$ATiO_2$ vs. 5–10 nm for Pt-$HTiO_2$, which is in agreement with the XDR results. Moreover, Figure 3c,f show that the Pt nanoparticles are well dispersed over the whole oxide surface in both samples. The average grain size of Pt nanoparticles (Figure 3g,h) formed during the photodeposition method was estimated from 100 metal deposits to be 3.4 ± 0.7 nm and 2.1 ± 0.5 nm for $ATiO_2$ and $HTiO_2$, respectively.

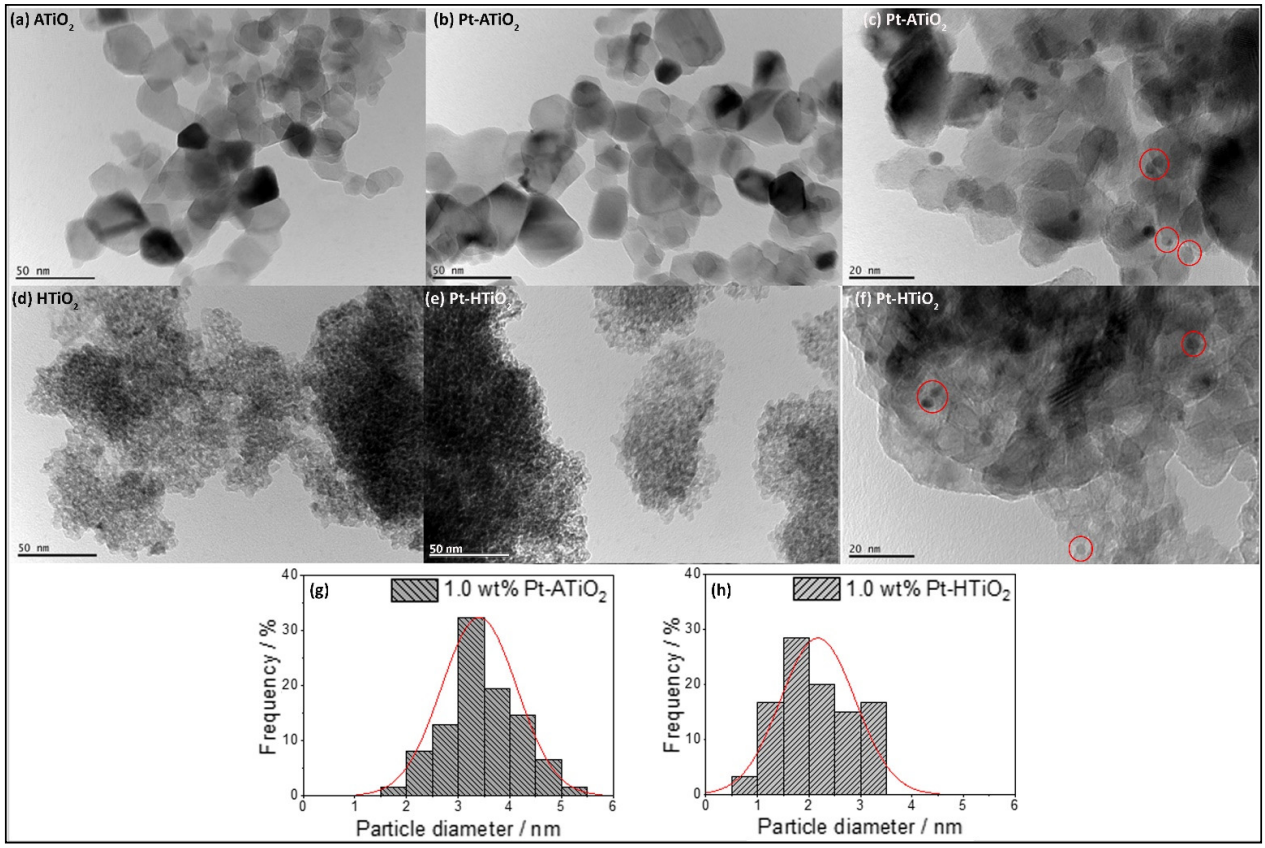

Figure 3. High-resolution transmission electron micrographs (HR-TEM) of pristine $ATiO_2$ (**a**), 1.0 wt% Pt-$ATiO_2$ (**b**,**c**), pristine $HTiO_2$ (**d**), and 1.0 wt% Pt-$HTiO_2$ (**e**,**f**). Pt particle diameter distribution images for 1.0 wt% Pt-$ATiO_2$ (**g**) and 1.0 wt% Pt-$HTiO_2$ (**h**).

2.2. Photocatalytic Reforming of Naphthalene

In this study, the same experimental conditions have been used to test the reforming of aqueous naphthalene solution employing different types of bare TiO_2 and platinized TiO_2 photocatalysts. It is worth to mention that no formation of molecular hydrogen was detected in the absence of light, or photocatalyst. Moreover, no activity for the H_2 evolution was observed during the illumination of pristine and platinized TiO_2 in the absence of naphthalene. This can be assigned to the fast recombination of the photogenerated charge carriers in the absence of a suitable hole scavenger, i.e., naphthalene, and the presence of an overpotential in the production of H_2 on the surfaces of the pristine photocatalysts [22].

Figure 4 presents the photocatalytic hydrogen evolution over two different commercial TiO_2 photocatalysts, $ATiO_2$ and $HTiO_2$, in their pristine forms and after their loading with different amounts of platinum NPs (0.5, 1.0, and 5.0 wt%). As depicted in Figure 4a,b, in the presence of naphthalene, both pristine photocatalysts are not efficient for photocatalyzed H_2, due to the higher overpotential of proton reduction [20] and to the insufficient transfer capacities of the photogenerated electrons to the absorbed species due to their trapping on the surface of TiO_2 as Ti^{3+} sites. The presence of platinum NPs on the surface of both TiO_2 photocatalysts activates the reaction of molecular hydrogen formation by reduces the overpotential for its formation, and due to the formation of Schottky junction at the interfaces of a Pt–TiO_2 composite, which reduces the rate of the charge carrier recombination [30]. Interestingly, Pt-$HTiO_2$ shows higher activity for H_2 production compared to Pt-$ATiO_2$ for all platinization ratios. Increasing the platinum deposition ratio on the surface of $HTiO_2$ from 0.5 to 1.0 wt% has no significant effect on the formation rate of molecular hydrogen. However, the 5.0 wt%. platinization ratio showed around 40% lower activity. On the other hand, the different Pt loading ratios on $ATiO_2$ revealed in the formation of the

same amounts of molecular hydrogen, indicating the independence of the Pt content on the activity in the case of $ATiO_2$.

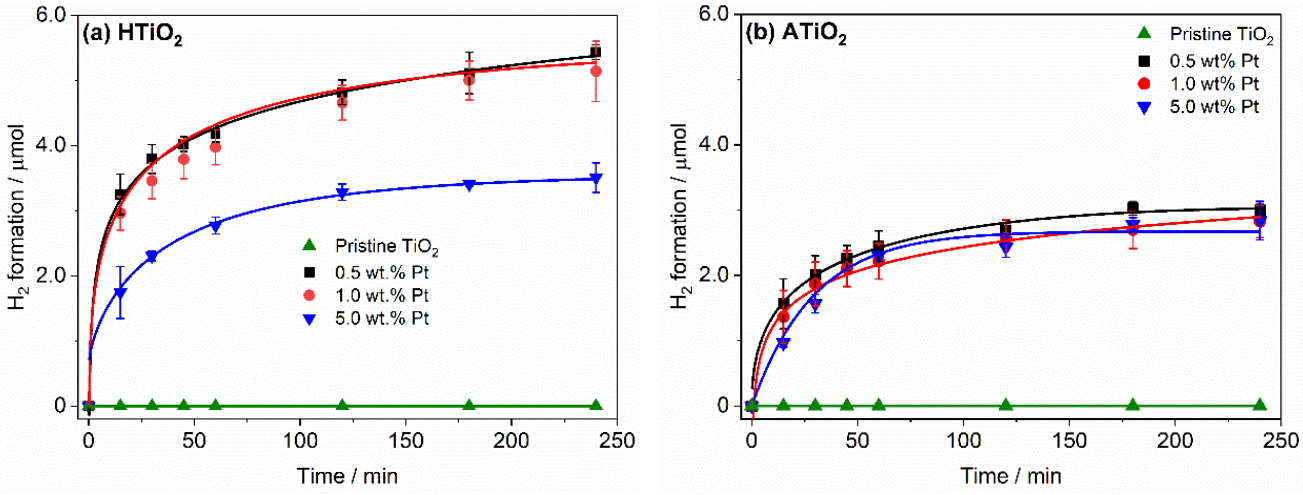

Figure 4. Comparison of molecular hydrogen formation during light-induced reforming of naphthalene in the presence of pristine TiO_2 and 0.5, 1.0, and 5.0 wt% Pt-TiO_2. (**a**) $HTiO_2$ and (**b**) $ATiO_2$ after 240-min illumination using simulated solar light. Photocatalyst mass concentration, 1 g L^{-1}; 156 µM aqueous solution of naphthalene.

The different H_2 formation between $ATiO_2$ and $HTiO_2$ could be explained by the enormous difference in the specific surface areas of these two catalysts because the photocatalytic process occurs on the photocatalyst surface. The larger the surface area, the higher the adsorption of the pollutant molecules due to the higher number of active sites (Ti^{4+}) on the TiO_2 surface. This leads to a rise in the rate of electron transfer to Pt nanoparticles and decreases in the internal mass transfer limitation of the pollutant to the active sites, thus promoting the H_2 formation [31,32].

Moreover, it is well known that the H_2 production is strongly dependent on the co-catalyst loading method, particle size, dispersion, and the oxidation state [33]. Since the same platinization method has been used and the TEM and XRD results confirm a well dispersion of Pt^0 NPs on the surfaces of both photocatalysts, we can exclude any effect of these factors. Besides, the larger particle size of Pt on the surface of $ATiO_2$ could imply a smaller surface area of the co-catalyst comparing to that for Pt-$HTiO_2$, which could decrease the H_2 formation rate [34]. If this is the case, we should observe an increase in the H_2 formation by increasing the Pt ratio from 0.5 to 1.0 wt% which compensates for this effect. However, this factor is excluded also, since the H_2 formation is almost the same.

On the other hand, we showed that upon increasing the fractional ratio of loaded Pt from 1.0 wt% to 5.0 wt%, the H_2 formation is reduced by 50%. The excessive loading amount of Pt on the surface of TiO_2 results in an increase of the opacity and, consequently, the light scattering of the suspension. This phenomenon reduces the number of photons absorbed by the TiO_2 particles and, thus, the number of charge carriers, thereby lowering the photocatalytic activity [35]. Besides, the decrease of the photocatalytic activity of the 5.0 wt% Pt-$HTiO_2$ can be attributed to the formation of dense larger islands. In fact, the growth of Pt nanocrystals under a high concentration of Pt precursor would be readily accelerated to form thicker and large Pt islands during the photodeposition process [36,37]. These dense islands negatively affect the H_2 formation due to the weak charge distribution between the platinum layers and the semiconductor [37]. Chen et al. [38] demonstrated that the charge redistribution occurs at the interfacial region between TiO_2 and the first Pt layer while the charge depletion/accumulation becomes negligible beyond the third layer.

Concomitantly, the photocatalytic oxidation of naphthalene solution in the absence of molecular oxygen (inert condition) was investigated employing the previous photocatalysts under the same experimental conditions. While the photolysis of naphthalene decreased

its initial concentration by ~33%, the use of photocatalyst enhanced the conversion ratio to 70–85% over pristine and platinized photocatalysts as shown in Figure 5. Pristine $ATiO_2$ exhibited higher photocatalytic performance for naphthalene conversion than did the pristine $HTiO_2$. This observation was expected, and it could be mainly ascribed to the fact that the recombination rate of the photoexcited *electron/hole* (e^-/h^+) pair in pristine $HTiO_2$ is faster. Anatase TiO_2 is generally reported as the most photochemically active phase of titania [39]. Compared to rutile, the anatase phase exhibits a 10-fold greater rate of hole trapping [40], which decreases the recombination rates of electron-hole pairs. Recently, by the means of combining theory and experiment, Scanlon and co-workers [41] suggested that the electron affinity of anatase is higher than that of rutile, leading to favor transfer the photogenerated electrons from rutile to anatase. This behavior has been previously suggested by Hurum et al. [42] who reported that Degussa P25 as a mixed phase of titania composed of small nanocrystallites of rutile dispersed within an anatase matrix possesses a higher activity than both pure phases. They affirmed that rutile acts as an antenna to extend the photoactivity into visible wavelengths and the stabilization of charge separation activates the catalyst, suppresses the recombination, and enhancing the photocatalytic activity.

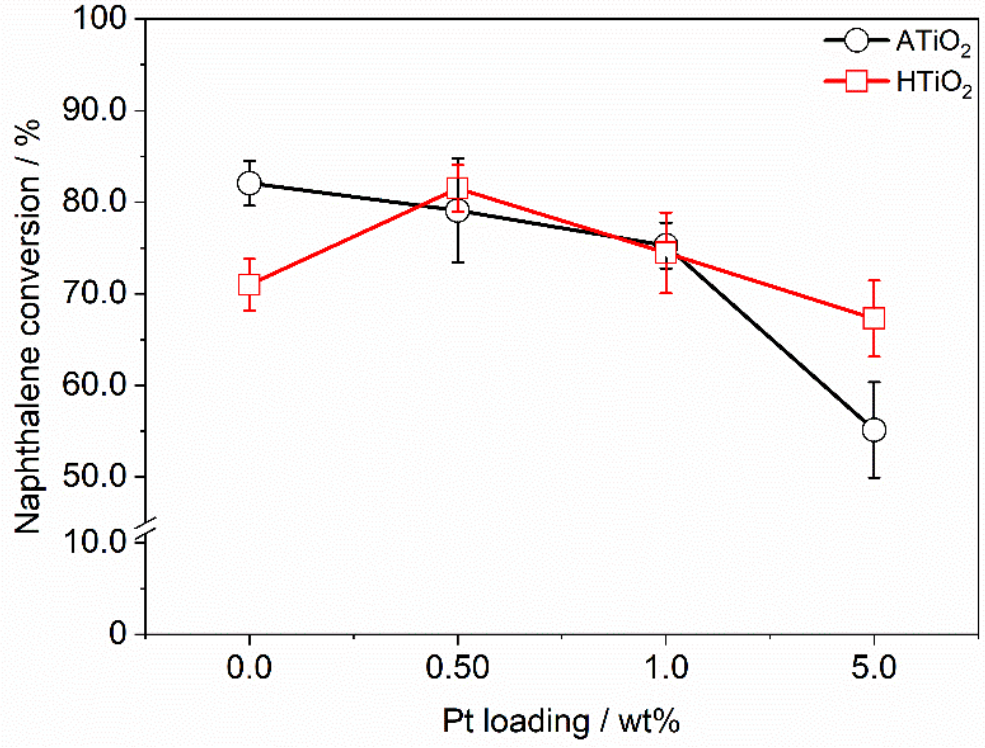

Figure 5. Naphthalene conversion in the presence of different photocatalysts. Conditions: [Naphthalene] = 0.156 mM, [catalyst] = 1 g L^{-1}, V = 15 mL, T = 25 °C, 240 min illumination under simulated solar light ($I_0 = 3.31 \times 10^{-4}$ mol m^{-2} s^{-1}).

Moreover, since the photocatalytic activity of the TiO_2 depends on its bulk and surface properties, it was suggested that the higher crystallinity leads to higher photocatalytic activity by reduces the charge carrier recombination [43]. Considering that TiO_2 photocatalyst exhibit either a high crystallinity and a low surface area or versa vise [44]. The XRD and TEM results in Figures 1 and 3 shown that $HTiO_2$ consists of small particles (8 nm) with very low crystallinity than $ATiO_2$. Thus, the low surface area of the P25 should be accompanied by higher crystallinity, which enhancing the photocatalytic efficiency.

Interestingly, loading platinum NPs on the surface of TiO_2 has two different behaviors related to the nature of the photocatalyst. Figure 5 shows that the photocatalytic conversion of naphthalene was decreased by increasing the platinum loaded ratio on $ATiO_2$. In fact,

increasing the platinum nanoparticles' content on the surface of pristine TiO_2 reduces the number of available active sites which plays a crucial role in the photooxidation of organic compounds [45]. This result is in good agreement with the work of Sun et al. [46] reporting that loading Degussa P25 with Pt resulted in a decrease of phenol decomposition and total carbon removal rates. The decrease of $ATiO_2$ activity after platinization suggests that Pt acts as a recombination center for the charge carrier. For such titania nanoparticles in aqueous media, Pt would not increase the efficiency of the charge carrier separation more than the separation already existing due to the presence of two mixed-phases. A recent report by Benz et al. [47] demonstrated that upon the trapping of the photogenerated electrons by the Pt islands on the surface of P25 in the absence of O_2, PT acts more as a recombination center regardless of its deposit ratio.

On contrary, the loading of platinum islands on the surface of $HTiO_2$ with a very small fraction (0.5 and 1.0 wt%) enhances the efficiency of the photocatalytic oxidation of naphthalene (Figure 5) compared to the use of pristine $HTiO_2$. Sun et al. [46] reported that the rates of phenol decomposition and the total carbon removal rose by a maximum factor of 1.5 when Hombikat TiO_2 was loaded with 1.0 wt% Pt. However, our data, as well as other reports [46,48], show that an optimum content of Pt (0.5–1.0 wt%.) on the surface of $HTiO_2$ should be considered, otherwise, increasing the Pt content reduces the efficiency of the photocatalytic process. In fact, the presence of hole scavengers (like naphthalene) can change the original equilibrium between the photogenerated holes and electrons. Platinum nanoparticles on the surface of TiO_2 act as electron scavengers, withdrawing the photogenerated holes out of the bulk TiO_2 because the formed Schottky barrier at Pt-TiO_2 interface serves as an efficient electron trap preventing the charge carrier recombination. This will enhance the charge carrier separation and prolong the lifespan of the photogenerated electrons [49]. However, increasing the Pt loading more than the optimum value leads to make the space charge layer very narrow and the penetration depth of light exceeds the space charge layer. Thus, platinum nanoparticles can act as recombination centers, where the electron-hole pairs recombination process will be favorable [48,50]. A more in-depth investigation of the Pt nanoparticles' effect on the dynamic charge carriers will be provided in Section 2.5.

In our previous report, we paid attention to the products generated from the photocatalytic reforming of naphthalene discussing their formation pathways by using different chromatographic techniques and isotopic substitution studies [14]. The hydroxylation of the aromatic ring was found to be the principal process in the photocatalytic reforming of naphthalene, which mainly produces 1-naphthalenol and 2-naphthalenol among others hydroxylated by-products. The possible pathway explaining the formation of the two naphthalenol's and molecular hydrogen is shown in Equations (1)–(7). The reforming of naphthalene is initiated by the excitation of the TiO_2, generating electrons and holes (Equation (1)), which either recombine or react with species present in the surrounding electrolyte. Naphthalene's oxidation occurs by a direct hole transfer, or indirectly via its reaction with a surface trapped hole ($-OH_S^{\cdot}$) by single electron transfer producing a naphthalene cation radical (Equation (2)). This carbocation radical reacts with water to form an OH adduct (Equations (3) and (4)), which is subsequently oxidized by another hole forming naphthalen-1-ol or naphthalen-2-ol (Equation (5)). On the other hand, the accumulated photogenerated electrons in the platinum nanoparticles reduce the adsorbed protons to hydrogen atoms (Equation (6)), which upon dimerization yields H_2 (Equation (7)).

$$TiO_2 \rightarrow n(e^- + h^+)TiO_2 \quad (1)$$

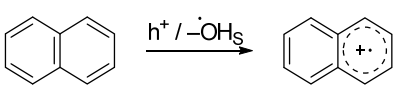

(2)

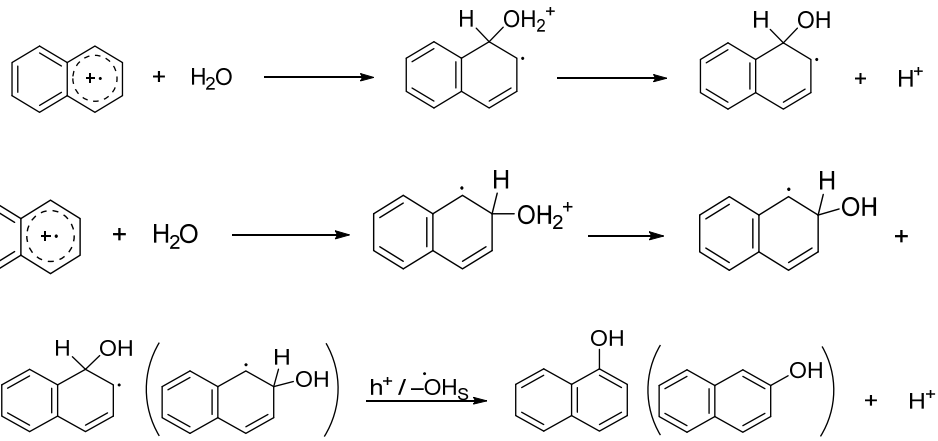

$$Pt - TiO_2\left[e^-\right] + H^+_{(ads)} \rightarrow Pt - TiO_2 + H^{\bullet}_{(ads)} \quad (6)$$

$$2H^{\bullet}_{(ads)} \rightarrow H_2(\uparrow) \quad (7)$$

In this context, we report in Figure 6 the detected amounts of these naphthalenols remaining in the reaction medium after 4 h of irradiation in the presence of all the synthesized Pt-TiO_2. Figure 6. shows that the accumulated amounts of 1-naphthalenol and 2-naphthalenol increased with increasing the Pt ratio on the surface of the different TiO_2 materials ($ATiO_2$ and $HTiO_2$). Platinization of the pristine TiO_2 enhance the formation of the naphthalenols products. While the relationship between the Pt content and the formation of naphthalenols is well established, there is an independency between their formation and the nature of TiO_2 when the same loading ratio was used.

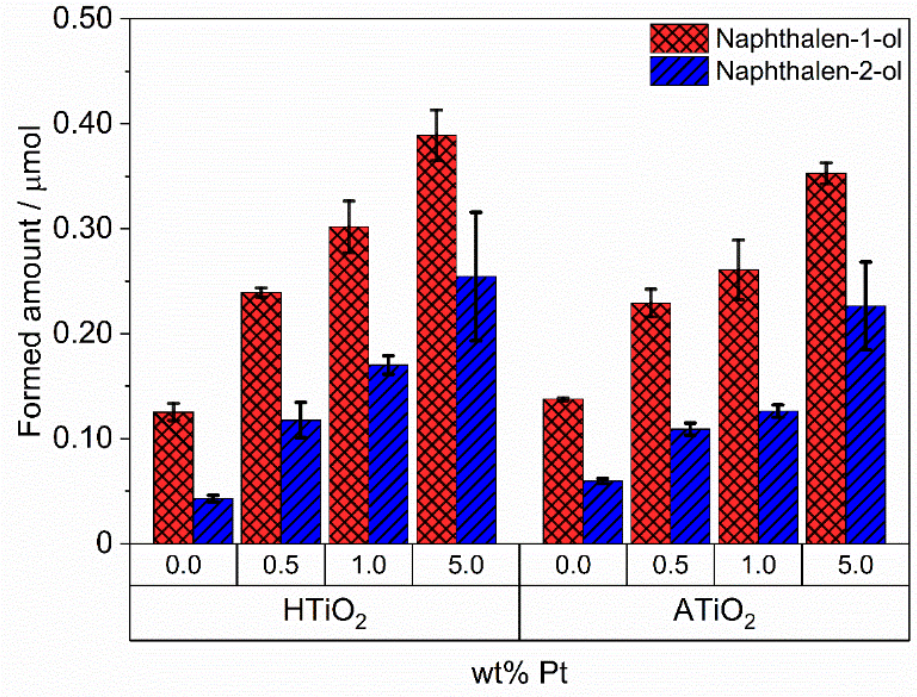

Figure 6. Photocatalytic formation of 1-naphthol and 2-naphthol during the reforming of naphthalene in aqueous suspensions of $HTiO_2$ and $ATiO_2$ loaded with various amounts of Pt.

Figures 4 and 6 confirm that the disappearance of the parent molecule naphthalene is accompanied by the formation of 1-naphthalenol and 2-naphthalenol besides the continu-

ous formation of H_2. In such a photocatalytic system, the lower detected amount of these by-products that accompanied with higher conversion of the mother compound should be an indication for increasing the formation rate of the H_2 (Equation (8)). However, this is not the case here, since we observed that all the synthesized Pt-ATiO$_2$ photocatalysts showed different photocatalytic activities towards the photooxidation of naphthalene and the formation of naphthalenols with almost the same amounts of evolved H_2. If we consider Equation (9) and the percentage of the total amount of naphthalenols to the converted naphthalene that is reported in Table 2, one can conclude that the formed amounts of H_2 for all the synthesis materials does not exceed 10–25% compared to the theoretical one. Thus, the concurrent decrease of the photocatalytic activity with the accumulation of the naphthalenols in the photocatalytic system by increasing the Pt ratio indicates the formation of other products. Such products can be strongly adsorbed on the surface of the photocatalysts and inhibiting the formation of H_2. It is reported that the photocatalytic oxidation of the aromatic compounds is initiated by the hydroxylation process producing different hydroxylated compounds as main products. This process is sometimes considered as the rate-determining step in the whole photocatalytic reaction under aerobic [51–53] and anaerobic conditions [19,54]. The strong adsorption of the surface phenoxy species and the coupling products on the available active sites [16,55–57], deactivates the surface of the photocatalyst and negatively affects both redox half photocatalytic reactions. This can be experimentally inferred by the decrease in the H_2 evolution rate after 30 min of irradiation with the simultaneous change in the photocatalyst color from light gray to faint brown. However, the color change is more pronounced in the case of Pt-ATiO$_2$, which can be reflected in the higher adsorbed amount of these products.

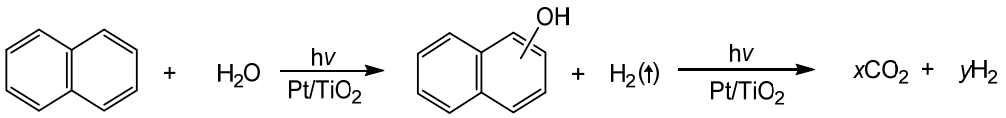

(8)

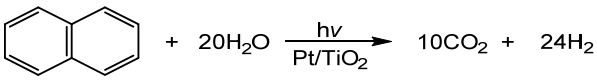

(9)

Table 2. Selectivity of total naphthalenols formation over different Pt-TiO$_2$ photocatalysts.

Photocatalyst / Property	HTiO$_2$			ATiO$_2$		
	0.5 wt% Pt	**1.0 wt% Pt**	**5.0 wt% Pt**	**0.5 wt% Pt**	**1.0 wt% Pt**	**5.0 wt% Pt**
Total naphthalenols selectivity %	22.4 ± 1.3	34.7 ± 2.4	46.2 ± 8.5	21.3 ± 1.2	27.3 ± 2.4	45.1 ± 4.4

2.3. Stability of Pt Deposit

The recyclability of the photocatalyst can provide a good indication that there is no relationship between the leaching of the co-catalyst and the decreasing of the photocatalytic activity during the reforming of naphthalene. Therefore, three consecutive recycling runs on the 0.5 wt% Pt-HTiO$_2$ were performed. The used photocatalyst was collected, irradiated in the presence of molecular oxygen for 60 min to remove the adsorbed organic compounds, washed with water, centrifugated, and then finally dried at 100 °C for 24 h.

As observed in Figure 7a,b, the reused photocatalyst exhibits good photocatalytic performance and stability over three cycles. Compared to the fresh photocatalyst, the naphthalene conversion efficiency remained almost the same, and a very slight decrease in molecular hydrogen formation was observed, which is considered within the experimental error. Furthermore, in order to check whether metal leaching takes place during the photocatalytic process, the Pt content in the Pt-HTiO$_2$ was analyzed after each photocatalytic cycle by means of the ICP-OES technique. The amount was found 20–25% lower than the original Pt ratio, mainly after the first cycle. In summary, one can conclude that

0.5 wt% Pt-UV100 is recyclable and stable. Therefore, the inhibition of H_2 formation and the naphthalene conversion during the photocatalytic process is not related to the leaching of the co-catalyst from the photocatalyst surface. These results support our hypothesis of the formation of stable photoformed products, which deactivate the photocatalyst surface.

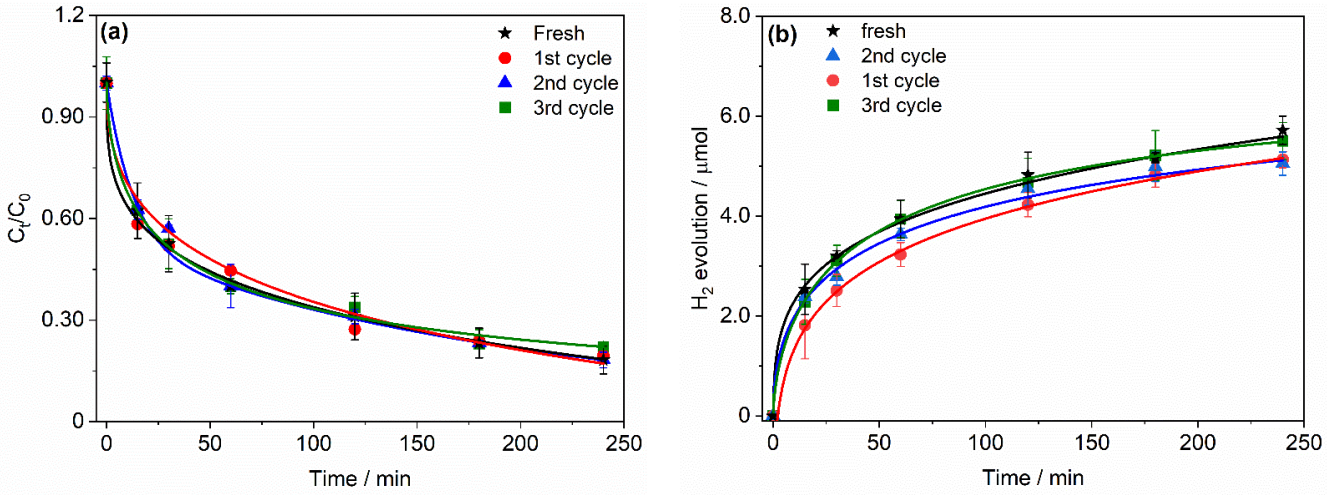

Figure 7. C_t/C_o for naphthalene conversion (**a**) and molecular hydrogen formation (**b**) during the photocatalytic reforming of naphthalene using recycled 0.5 wt% Pt-$HTiO_2$ photocatalyst. Conditions: [Naphthalene] = 0.156mM, [catalyst] = 0.5 g L^{-1}, T = 25 °C, 240-min illumination under simulated solar light.

Moreover, since the decrease of the Pt content during the recyclability experiments is not affecting the H_2 formation and the conversion of naphthalene. Thus, another important aspect can be concluded from these results: the 0.5 wt% of Pt loaded on $HTiO_2$ might not be the optimum loaded ratio. Although many previous studies have reported that 0.5 wt% is the optimum ratio of loaded Pt on the TiO_2 [44], other reports have shown different values either higher [48] or lower [19,20] than 0.5 wt% Pt. Therefore, a further investigation in the range lower than 0.5 wt% is required to avoid an excess of the valuable Pt metal, thus, decreasing the cost of this photocatalyst in case of its practical application.

2.4. Effect of Naphthalene Oxidation Products on the H_2 Evolution

It is widely accepted that the formation of the by-products presumably causing inhibition of H_2 production during the photocatalytic reforming of the organic compounds [57,58]. We examine the validity of this hypothesis by performing different photocatalytic experiments using naphthalene, 1-naphthalenol, and 2-naphthalenol under the same experimental conditions. The photooxidation profiles of the three compounds as a function of irradiation time are shown in Figure 8a. Apparently, the photooxidation of naphthalene is higher than that for both naphthalenol compounds. After 240 min of illumination, the conversion of naphthalene, naphthalen-1-ol, and naphthalen-2-ol were found to be 75%, 63%, and 52%, respectively. All the tested compounds showed a faster conversion rate in the initial stage of the reaction, which is attributed to the abundant availability of active sites on the surface of TiO_2 [59]. In this stage, naphthalene shows the longest period (60 min) with the faster conversion rate, while, the shorted period (15 min) with the slowest rate was observed for naphthalen-2-ol. The initial photonic efficiencies of the photooxidation of these compounds after 60 min of illumination was found to be 0.14 ± 0.01%, 0.1 ± 0.02%, and 0.08 ± 0.01% for naphthalene, naphthalen-1-ol, and naphthalen-2-ol, respectively. A noticeable inhibition in the conversion rates was recorded after the first rapid period to reach a steady-state stage after 120 min. This behavior has been observed by S.M. King et al. [60], who reported that the initial stage was found to be the most rapid photodegradation rate for PAH removal in the presence and the absence of the photocatalyst.

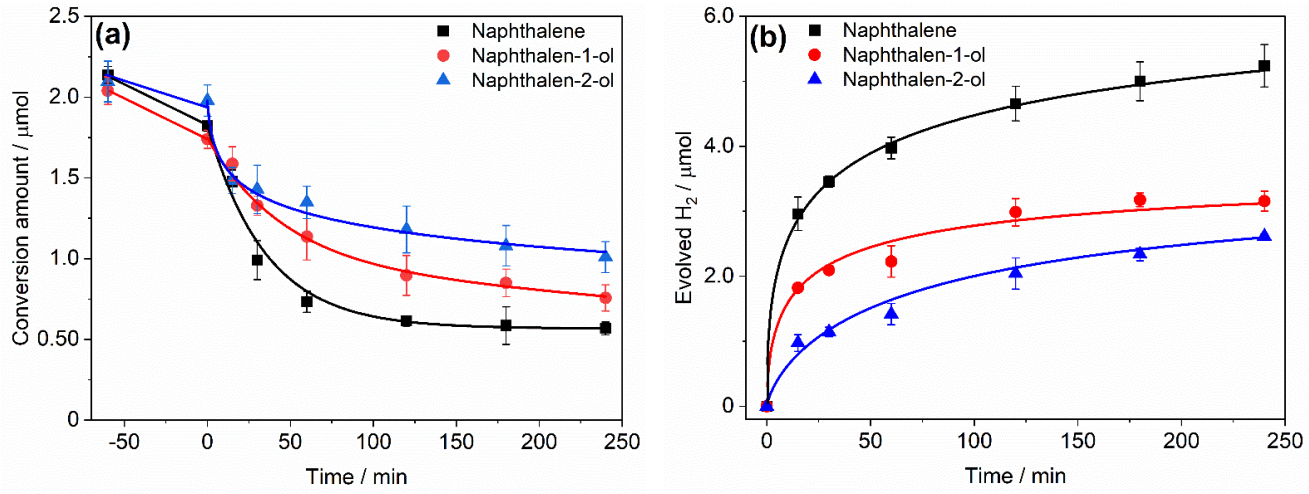

Figure 8. Photooxidation (**a**) and molecular hydrogen formation (**b**) during the photocatalytic reforming of naphthalene, naphthalen-1-ol, and naphthalen-2-ol as a function of illumination time. Conditions: [Naphthalene] = 2.1 µmol, [naphthalenols] = 2.1 µmol, [catalyst] = 1 g L^{-1} 1.0 wt% Pt-HTiO_2, T = 25 °C, illumination under simulated solar light.

On the other hand, a similar trend was observed for the photocatalytic H_2 formation profile shown in Figure 8b. Naphthalene exhibits a two-fold higher formation amount of H_2 after irradiation for 240 min. One more time, the faster formation rate was observed during the first stage of the reaction, i.e., during the first 60 min. Afterward, all the tested compounds exhibit almost a similar formation rate. The initial photonic efficiencies for the H_2 evolution in the first stage was found to be 0.51 ± 0.02%, 0.28 ± 0.03%, and 0.18 ± 0.02% for naphthalene, naphthalen-1-ol, and naphthalen-2-ol, respectively.

We reported previously that naphthalene is oxidized into CO_2, H_2, and other by-products, such as naphthalenols, coupling, and hydroxylated compounds [14]. At the beginning of the photocatalyst process, the concentrations of these organic products are very low in the system. Naphthalene is efficiently oxidized on the clean surface of the TiO_2 since there is no competition from these products to the surface of the photocatalyst. However, during the reaction, the formed intermediates are accumulated in the system and subsequently oxidized to other more polar compounds such as polyhydroxylated, quinones, and organic acid products [14,61,62]. Such products have higher polarity comparing to naphthalene, therefore they can strongly adsorb to the surface of the photocatalyst, blocking the active sites on the catalyst surface. In general, the degradation of these compounds leaves recalcitrant carbonaceous residues on the photocatalyst surface as a result of incomplete degradation [63,64], especially in the absence of O_2, which decreasing the photocatalytic activity of the TiO_2.

In this respect, it is noteworthy that the adsorption of the organic molecules is a very important factor in the photocatalytic process, however, in some cases, the strong adsorption of the organic compounds or intermediates may act as poison for the catalyst surface, which enhances the charge carrier recombination. The strong multilayer adsorption of organic molecules around the catalyst particles could lead to the excitation of these compounds by absorbing a significant amount of solar light rather than the photocatalyst. This could limit the interaction between the incoming light and the photocatalyst in the case of the indirect photooxidation mechanism, which reduces the photocatalytic efficiency [65,66]. In our case, the lack of naphthalen-2-ol photooxidation after less than 30 min of irradiation can be related to the adsorption of stable photoformed products on the surface of the photocatalyst that hinders the photocatalytic process. The photocatalytic degradation of 2-naphthol was investigated by Qourzal et al. [67] with and without replenishing the O_2 in the system and was found to be 100% and 58%, respectively. Our results suggest that the different kinds of organic pollutants have a significant influence on the photocatalytic H_2 production and the simultaneous photocatalytic degradation of the organic pollutant. In

our case, the differences in the photonic efficiencies of the photooxidation and H_2 evolution can be related to the different photocatalytic behavior of these compounds. According to Denny et al. [68], increasing the number of hydroxyl groups in aliphatic compounds increases mineralization, however, this effect was not evident for the hydroxylated aromatic compounds. On the other hand, many reports have been shown that the photoreforming of aromatic hydrocarbons is more reactive than hydroxylated aromatic compounds [18]. Since the photocatalytic reforming of naphthalene is more efficient than both naphthalenols compounds under the same experimental conditions, our results thus confirm this hypothesis. Therefore, based on the presented results, we can conclude that the photocatalytic process is highly dependent on the nature of the organic compound.

2.5. EPR Study

EPR spectroscopy is a suitable technique for studying charge carrier separation to predict the photocatalytic activity of different photocatalysts. All the EPR analyses (Figure 9) were carried out on 1.0 wt% Pt-ATiO$_2$ and 1.0 wt% Pt-HTiO$_2$ in the N_2 atmosphere to avoid the contribution from any other electron scavenger, i.e molecular oxygen. Thus, to investigate the effect of the photocatalyst nature and the loaded PtNPs on the photogenerated electron and hole paramagnetic species, the signals from both photocatalysts were acquired before and after UV-Vis irradiation. Very weak signals observed for both catalysts in the dark can be related to formed oxygen vacancies during preparation. While under illumination, both photocatalysts exhibit two major features, i.e., the signals from the surface trapped holes at $g > 2.000$, and the signals from the trapping of electrons at $g < 2.00$, as shown in Figure 9a,b [69,70]. Irradiation of the platinized TiO_2 samples by the light of higher energy than the respective bandgap, lead to the formation the e^- - h^+ *pair*, as shown in Equation (1). Both e^- and h^+ can be trapped on the surface or interior of the lattice. The conduction band electrons can be trapped on the Pt islands and Ti^{IV} ions. In the second case, they form a paramagnetic Ti^{III} in the bulk or the surface [71,72]. On another hand, the valance band trapped holes can be located on O^{-2} as a O^- either in the surface or subsurface [70,72]. Shapovalov et al. [73] suggested that the holes can be delocalized over at least two surface oxygen atoms, and can be transferred between surface oxygen atoms and adsorbed species, thus, both OH and O^- species can be formed.

The hole trapping site in Figure 9a at g-tensor components $g_x = 2.004$, $g_y = 2.015$, and $g_z = 2.019$, represent the fingerprint of anatase oxygen site, while the small-signal at $g_\perp = 1.992$ and the shoulder at $g_\parallel = 1.965$ are assigned for the anatase lattice trapping electron site as Ti^{+3} [70,74]. On other hand, the trapped holes signals of Pt-ATiO$_2$ in Figure 9b at g-tensor components $g_x = 2.003$, $g_y = 2.019$, and $g_z = 2.026$ are not sufficiently resolved, which is considered a combination of trapped oxygen sites from anatase and rutile. However, the lattice trapped electron's EPR signals are well resolved. The Ti^{+3} signal from anatase can be observed clearly at the same g-tensor components assigned in Figure 9a, while the remaining signals at $g_\perp = 1.980$ and $g_\parallel = 1.945$ are characteristics for Ti^{+3} sites for trapped electrons in the rutile lattice [69,74].

Figure 9a,b clearly show around 20% higher relative intensity of trapped holes in Pt-HTiO$_2$ (determined by double integration of the corresponding signal [75]) than those in Pt-ATiO$_2$. On the other hand, Pt-ATiO$_2$ exhibits the strongest electron signals at both Ti^{+3} sites. Since no hole scavenger was used, the increase in the Ti^{3+} EPR signals can be a monitor of a potential increase in the charge carrier recombination during the photocatalytic processes, since the trapped electrons in the lattice will recombine with the photogenerated holes. These results indicate that Pt-HTiO$_2$ yields a better electron transfer to Pt islands than Pt-ATiO$_2$. Thus, an efficient charge carrier separation in the case of Pt-HTiO$_2$ is expected, which inhibits the electron-hole recombination and increases the photocatalytic efficiency.

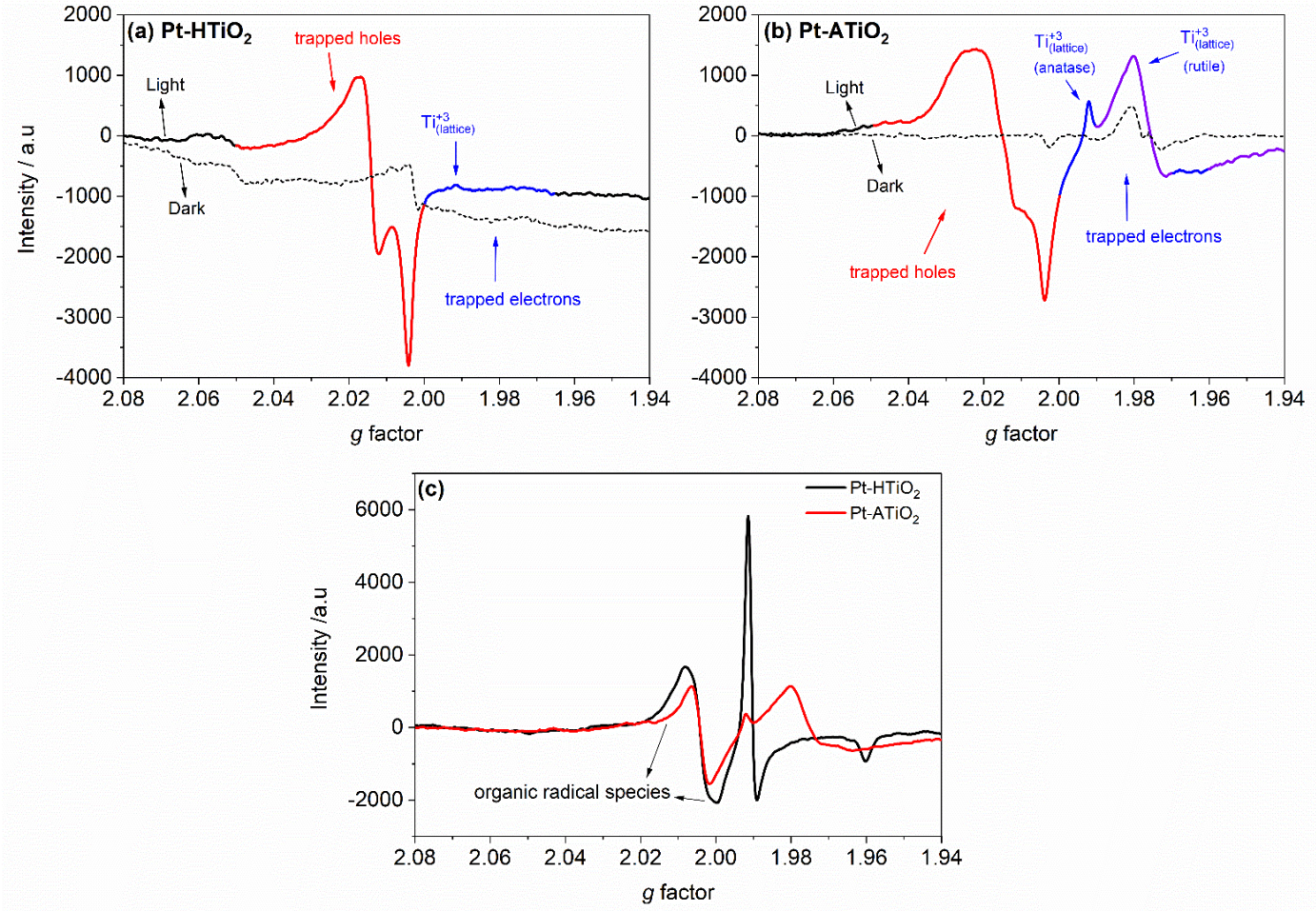

Figure 9. EPR spectra measured at 77 K in N_2 atmosphere for (**a**) 1.0 wt% Pt-$HTiO_2$, and (**b**) 1.0 wt% Pt-$ATiO_2$ in dark (dash line) and light (solid line). (**c**) The photogenerated signals for 1.0 wt% Pt-$HTiO_2$ (black line) and 1.0 wt% Pt-$ATiO_2$ (red line) in the presence of N_2-naphthalene vapor under illumination.

Moreover, to investigate the different mechanisms of generating organic radicals by the photogenerated holes, experiments were performed in the presence of naphthalene as a hole scavenger. Upon the irradiation of both platinized TiO_2 samples, the photogenerated holes react with naphthalene, forming the naphthalene radical cation via single-electron transfer (Equation (2)) [14].

The EPR spectra in Figure 9c show that both photocatalysts generate similar signals having g-tensor components $g_x = 2.002$, $g_y = 2.006$, related to the formation of naphthalene radical cation [42], which formed as a result of the reaction between naphthalene and the photogenerated holes. Pt-$HTiO_2$ produces a relatively higher intense signal of such organic radicals and a stronger signal of the trapped electrons (Ti^{+3}) compared to both signals produced from Pt-$ATiO_2$. This could be attributed to the higher amount of the tapped holes that are available to react with the adsorb naphthalene, due to the efficient charge carrier separation in the Pt-$HTiO_2$ photocatalyst. Interestingly, unlike Pt-$HTiO_2$, the intensity of the trapped electrons produced from Pt-$ATiO_2$ (Ti^{+3} anatase and rutile) does not change upon the introduction of naphthalene as a hole scavenger. The higher intensity of the formed organic radicals in Pt-$HTiO_2$ would be accompanied by a higher amount of the photogenerated electrons, which can be partially collected by PtNPs on the surface of Pt-$HTiO_2$ to catalyze the reduction of H^+ ions to H_2, while the remaining electrons can be trapped as Ti^{III}.

Furthermore, the $Ti^{+3}_{(lattice)}$ signals intensity in Pt-$ATiO_2$ is relatively low than the respective signal intensity in Pt-$HTiO_2$. This can be related to the rapid transfer of the

photogenerated electrons from the $ATiO_2$ to the Pt islands. If so, we should observe a relatively higher signal from formed organic radicals. However, a relatively lower signal was observed, which can be attributed to faster recombination between photogenerated electrons and holes, results in a decrease in the amounts of evolved H_2 during the reforming of naphthalene. According to Sun et al. [46], the interfacial contact between the two phases (rutile and anatase) in Pt-TiO_2 (P25) leads to the band bending, which increases the anatase conduction band energy within the space charge layer. Therefore, prohibiting the photogenerated electrons from migrating from anatase to rutile. On the other hand, the valance band bending results in the migration of the holes from the anatase to the rutile valance band [41]. However, since the mobility and diffusivity of the electrons, as well as the electron flux in the rutile phase is very low compared to anatase, the electrons flux from anatase to rutile, if happened, is negligible [41,46]. Therefore, trapped holes are accumulated in rutile particles, and electrons are left in the anatase, where the oxidation and reduction mainly take place, respectively. However, the slow movement of the rutile electrons enhanced the probability of the electron−hole recombination, decreasing the rutile's activity. Hence, it is suggested that the formed charge carriers in the rutile phase of P25 do not improve the photoactivity a lot, instead, it plays a role of charge carrier separation and provides sites for oxidation [76].

3. Experimental

3.1. Materials

Titanium dioxide, Aeroxide P25 ($ATiO_2$) consist of anatase/rutile mixture was supplied from Evonik Corporation, USA and Hombikat UV100 ($HTiO_2$) pure anatase phase was supplied by Sachtleben Chemie GmbH. Naphthalene (≥99.0%), naphthalen-1-ol (97%), naphthalen-2-ol (99%), and chloroplatinic acid hexahydrate ($H_2PtCl_6 \cdot 6H_2O$, 99.9%) were purchased from Sigma-Aldrich. Methanol HPLC gradient grade was purchased from Carl-Roth. All chemicals were used as received without any further purification, and their solutions were prepared with deionized water obtained from a Millipore Mill-Q system (18.2 MΩ.cm, 25 °C).

3.2. Preparation of the Pt-TiO_2 Photocatalysts

Platinum-loaded TiO_2 samples were prepared by a photodeposition method according to our previous report [14]. A 1.5 g of the commercially available TiO_2 (UV100 or P25) was dispersed into 150 mL of 10% aqueous methanol solution with the desired amount of platinum precursor (H_2PtCl_6, 0.1 M) corresponding to obtain 0.5, 1.0, and 5.0 wt% of Pt-TiO_2 nanoparticles. The suspension stirred for 1 h and then purging for another 1 h with argon. Afterward, it was top illuminated for 4 h with UV(A) light employing a Philips CLEO lamp inside a climatic chamber at 18 °C. The solid was then collected by centrifugation, repeatedly washed one time with methanol, fourth with distilled water, and finally dried at 100 °C for 24 h.

3.3. Photocatalytic Experiments

The photocatalytic activity of the Pt-$ATiO_2$ and Pt- $HTiO_2$ were evaluated through the photocatalytic reforming of naphthalene, carried out in a batch mode using 20 mL glass vials tightly closed with a crimp cap and silicon septum. Due to the experiment limitation, the evaporation and lower solubility of naphthalene during the preparation step [8], a fresh, saturated deaerated stock solution from it was prepared before each photocatalytic experiment. The estimated concentration of this solution is about 2.44×10^{-4} mol L^{-1} at 25 °C, while, the specific concentration was determined by using the HPLC-UV technique.

In a typical experiment, 15 mg of the photocatalyst powder was suspended in a specific amount of deionized water. The vials were closed with the crimp septum and purged with argon for 30 min. Afterward, the desired volume from the naphthalene stock solution was injected inside the 15 mL-reaction vials using a pre-purged (with argon gas) needle syringe to have a final concentration of 20 mg L^{-1} (1.56×10^{-4} mol L^{-1} at 25 °C). Finally,

the vials were left in the dark inside an orbital shaker for 1 h to reach the equilibrium adsorption. The orbital shaker was placed at a 30 cm distance below a 1000 W xenon lamp (Hönle UV Technology, Sol 1200) equipped with a filter to simulate the solar light. The temperature of the vials was controlled at 25 ± 2 °C by using a water bath. It is worth to mention that the reported concentrations of naphthalene in wastewater range between ng L^{-1} to μg L^{-1} [77,78], which are considered very low concentrations compared to those that were used in the photocatalytic experiments. Such a higher concentration was used to ensure proper repeatability in all experiments and to avoid the problem of naphthalene evaporation. Furthermore, almost a complete removal of naphthalene was observed by using a concentration lower than 20 ppm [79], which will prevent a logical and practical comparison between the performance of both photocatalysts.

The photon flux density was measured from the spectral irradiance of the lamp in the wavelength range between 320 nm and 380 nm and was found to be $I_0 = 3.31 \times 10^{-4}$ mol m^{-2} s^{-1}. The photonic efficiencies were calculated based on Equation (10) [26].

$$\xi = \frac{\text{degradation or formation rate } \left(\text{mol s}^{-1}\right)}{\text{photon flux } \left(\text{mol m}^2\ \text{s}^{-1}\right)} = \frac{N_A hc\ V\Delta C}{I\lambda A\Delta t} \quad (10)$$

where V is the suspension volume (0.015 l), $\Delta C/\Delta t$ is the formation rate (mol s^{-1}), A is the illuminated area (6.60×10^{-4} m^2), I is the light intensity (Wm^{-2}), λ is the corresponding wavelength (m), N_A is the Avogadro's constant (6.023×10^{23} mol^{-1}), h is the Planck constant (6.636×10^{-34} W s^2) and c is the velocity of light (3.00×10^8 m s^{-1}).

To quantify the photocatalytically evolved H_2, a 50 μL gas sample was periodically taken from the reaction headspace using a Valco gas-tight sampling syringe and injected into a Shimadzu 8A gas chromatograph (GC). The GC was equipped with a thermal conductivity detector (TCD) and a stainless- molecular sieve 5A GC column (Sigma-Aldrich, St. Louis, MO, USA). The temperatures of the column, injector port, and TCD detector were maintained at 80 °C, 120 °C, and 120 °C, respectively.

The concentration of naphthalene before and after the experiment was quantified using Merck L 6200A (Hitachi) High-Performance Liquid Chromatography (HPLC) system equipped with a Nucleosil 120 C18 (250 mm × 4.0 mm × 5.0 μm) column and a UV-VIS detector operated at 276 nm. The column temperature was maintained at 30 ºC. The mobile phase was a mixture of methanol (A) and water (B) with a gradient mode [initial (40% A: 60% B); 17 min (85% A: 15% B) and hold for 4 min; 2 min (95% A: 5% B) and hold for 4 min; and finally, 1 min (40% A: 60% B) and hold for 3 min]. The flow rate was 1.0 mL min^{-1} and the injection volume was 50 μL. The total run time was 32 min. A 1 mL from each reaction vial was taken at the end of the experiment, filtrated through 0.2 μm PTFE syringe filters to remove the TiO_2 particles, and then injected immediately in the HPLC to avoid the loss of naphthalene from the solution.

3.4. Catalyst Characterization

The synthesized photocatalysts were characterized by X-ray diffraction analysis (XRD) patterns using Bruker D8 Advance diffractometer (Bruker AXS GmbH) with a Bragg-Brentano geometry employing Cu Ka radiation (λ = 1.54060 Å). The patterns were recorded in the 2θ range between 10° and 80° in steps of 0.039°. Brunauer–Emmett–Teller (BET) specific surface areas were measured by a FlowSorb II 2300 instrument equipped with a Micromeritics AutoMate 23. Prior to the measurements, all the synthesized platinized TiO_2 samples were pre-degassed in a vacuum at 150 °C for 1 h. The specific surface area was measured in triplicates and determined through single-point standard BET surface area measurements. Diffuse reflectance (DR) UV-vis spectra were recorded with a Varian Cary 100 Bio Spectrophotometer (Agilent), equipped with a diffuse reflectance accessory. $BaSO_4$ was used as a baseline and blank for measuring the wavelength range from 200 to 800 nm. The actual percentage of Pt nanoparticles on the TiO_2 surface was determined

by using Inductively coupled plasma—optical emission spectrometry (ICP-OES, Varian 715-ES, Varian). A 20 to 30 mg of the Pt-TiO_2 samples were digested at 150 °C for 3h in 5.00 mL aqua regia (3:1 HCl/HNO_3 mixture) until the acid nearly evaporated. Afterward, the digested samples re-dissolved in 10.00 mL of 3% HNO_3 and filtrated through a filter paper. The eluent was stored at 4 °C prior to the analysis. The 3% HNO_3 was used as a blank for all the analyses. The results are summarized in Table 1. Transmission Electron Microscopy (TEM) measurements were carried out on a Tecnai G2 F20 TMP (FEI) with an acceleration voltage of 200 kV field emission gun (FEG). The powdered specimen was dry fixed on a holey carbon film supported by a Cu grid.

3.5. EPR In Situ Experiments

Electron paramagnetic resonance (EPR) spin trapping technique was applied to study the dynamic of the charge carrier by monitoring the formation of paramagnetic intermediates upon irradiation of different platinized TiO_2 materials in situ using an X-band EPR MiniScope MS400 (Magnettech GmbH, Berlin, Germany) spectrometer. The experiments were carried out at 77 K using liquid nitrogen. The solid materials were charged inside an EPR quartz tube (260 mm × 4.0 mm × 0.5 mm), purged once with N_2, and other with N_2-naphthalene vapor mixture for 30 min each for separate measurements. The instrument was operated at 9.43 GHz field modulation and equipped with a UV spot-light (LC8, Hamamatsu, 200 W super-quiet mercury-xenon lamp). The acquisition parameters were as follows: center field: 337.07 mT, sweep time 30 s, range 30 mT, number of points: 4096, number of scans: 1, modulation amplitude: 0.15 mT, power: 10 mW, and gain: 5.

4. Conclusions

In summary, the presented results show that Pt-$HTiO_2$ exhibits a higher photocatalytic activity for H_2 evolution than Pt-$ATiO_2$ during the photoreforming of the naphthalene. However, both platinized photocatalysts show a similar activity towards the photooxidation of naphthalene. The 0.5 wt% fractional ratio of Pt nanoparticles on the surface of the $HTiO_2$ shows the higher photocatalytic activity toward the naphthalene conversion and H_2 evolution, while no relation was found between the H_2 evolution and the Pt content on the $ATiO_2$. In the presence of the hole scavenger naphthalene, Pt nanoparticles on the surface of $HTiO_2$ act as electron scavengers, enhancing hydrogen production rates, while on the surface of $ATiO_2$ they act as recombination centers for the photogenerated charge carrier. The photoreforming of naphthalene over Pt-$HTiO_2$ resulted in higher amounts of H_2 and conversion compared to their corresponding intermediates, naphthalen-1-ol and naphthalen-2-ol. The inhibition of the H_2 formation and naphthalene conversion rates during the photocatalysis process is ascribed to the adsorption of the formed intermediates on the surface of the TiO_2. Although this technique is considered as a promising process for hydrogen evolution along with naphthalene degradation, cheaper traditional removal techniques may be more appropriate because of the low concentrations of naphthalene in real wastewaters.

Author Contributions: Conceptualization, methodology, formal analysis, investigation, writing—original draft preparation, O.A.-M.; writing—review and editing, O.A.-M., Y.A. and R.D.; supervision, R.D. and D.W.B. All authors have read and agreed to the published version of the manuscript.

Funding: Financial support from the Global Research Laboratory Program (2014 K1 A1 A2041044), Korea Government (MSIP) through NFR is gratefully acknowledged.

Institutional Review Board Statement: Not applicable.

Informed Consent Statement: Not applicable.

Data Availability Statement: The data presented in this study are available on request from the corresponding author.

Acknowledgments: Financial support from the Katholischer Akademischer Ausländer-Dienst (KAAD) and Graduiertenakademie at Gottfried Wilhelm Leibniz Universität Hannover are gratefully acknowledged for providing scholarships for Osama Al-Madanat to perform his O. Al-Madanat wishes to thank Mariano Curti for the helpful assistance and discussion while preparing the manuscript. The publication of this article was funded by the Open Access Publishing Fund of Leibniz Universität Hannover.

Conflicts of Interest: The authors declare no conflict of interest.

References

1. Møller, K.T.; Jensen, T.R.; Akiba, E.; Li, H.-W. Hydrogen—A sustainable energy carrier. *Prog. Nat. Sci.* **2017**, *27*, 34–40. [CrossRef]
2. Niaz, S.; Manzoor, T.; Pandith, A.H. Hydrogen storage: Materials, methods and perspectives. *Renew. Sust. Energ. Rev.* **2015**, *50*, 457–469. [CrossRef]
3. Cavendish, H., XIII. Experiments on air. *Philos. Trans. R. Soc.* **1784**, *74*, 119–153. [CrossRef]
4. Kennedy, J.; Bahruji, H.; Bowker, M.; Davies, P.R.; Bouleghlimat, E.; Issarapanacheewin, S. Hydrogen generation by photocatalytic reforming of potential biofuels: Polyols, cyclic alcohols, and saccharides. *J. Photochem. Photobiol. A* **2018**, *356*, 451–456. [CrossRef]
5. Fajrina, N.; Tahir, M. A critical review in strategies to improve photocatalytic water splitting towards hydrogen production. *Int. J. Hydrog. Energy* **2019**, *44*, 540–577. [CrossRef]
6. Al Nasir, F.; Batarseh, M.I. Agricultural reuse of reclaimed water and uptake of organic compounds: Pilot study at Mutah University wastewater treatment plant, Jordan. *Chemosphere* **2008**, *72*, 1203–1214. [CrossRef]
7. Rubio-Clemente, A.; Torres-Palma, R.A.; Penuela, G.A. Removal of polycyclic aromatic hydrocarbons in aqueous environment by chemical treatments: A review. *Sci. Total Environ.* **2014**, *478*, 201–225. [CrossRef]
8. Wauchope, R.D.; Getzen, F.W. Temperature dependence of solubilities in water and heats of fusion of solid aromatic-hydrocarbons. *J. Chem. Eng. Data* **1972**, *17*, 38–41. [CrossRef]
9. Ghasemi, N.; Gbeddy, G.; Egodawatta, P.; Zare, F.; Goonetilleke, A. Removal of polycyclic aromatic hydrocarbons from wastewater using dual-mode ultrasound system. *Water Environ. J.* **2020**, *34*, 425–434. [CrossRef]
10. Kadri, T.; Rouissi, T.; Kaur Brar, S.; Cledon, M.; Sarma, S.; Verma, M. Biodegradation of polycyclic aromatic hydrocarbons (PAHs) by fungal enzymes: A review. *J. Environ. Sci.* **2017**, *51*, 52–74. [CrossRef]
11. Chu, L.B.; Yu, S.Q.; Wang, J.L. Gamma radiolytic degradation of naphthalene in aqueous solution. *Radiat. Phys. Chem.* **2016**, *123*, 97–102. [CrossRef]
12. Mondal, K.; Bhattacharyya, S.; Sharma, A. Photocatalytic degradation of naphthalene by electrospun mesoporous carbon-doped anatase TiO_2 nanofiber mats. *Ind. Eng. Chem. Res.* **2014**, *53*, 18900–18909. [CrossRef]
13. Garcia-Martinez, M.J.; Canoira, L.; Blazquez, G.; Da Riva, I.; Alcantara, R.; Llamas, J.F. Continuous photodegradation of naphthalene in water catalyzed by TiO_2 supported on glass Raschig rings. *Chem. Eng. J.* **2005**, *110*, 123–128. [CrossRef]
14. Al-Madanat, O.; Alsalka, Y.; Curti, M.; Dillert, R.; Bahnemann, D.W. Mechanistic insights into hydrogen evolution by photocatalytic reforming of naphthalene. *ACS Catal.* **2020**, *10*, 7398–7412. [CrossRef]
15. AlSalka, Y.; Hakki, A.; Fleisch, M.; Bahnemann, D.W. Understanding the degradation pathways of oxalic acid in different photocatalytic systems: Towards simultaneous photocatalytic hydrogen evolution. *J. Photochem. Photobiol. A* **2018**, *366*, 81–90. [CrossRef]
16. Weon, S.; Kim, J.; Choi, W. Dual-components modified TiO_2 with Pt and fluoride as deactivation-resistant photocatalyst for the degradation of volatile organic compound. *Appl. Catal. B-Environ.* **2018**, *220*, 1–8. [CrossRef]
17. Schneider, J.; Bahnemann, D.W. Undesired Role of Sacrificial Reagents in Photocatalysis. *J. Phy. Chem. Lett.* **2013**, *4*, 3479–3483. [CrossRef]
18. Hashimoto, K.; Kawai, T.; Sakata, T. Photocatalytic reactions of hydrocarbons and fossil-fuels with Water—Hydrogen-production and oxidation. *J. Phys. Chem.* **1984**, *88*, 4083–4088. [CrossRef]
19. Yuzawa, H.; Aoki, M.; Otake, K.; Hattori, T.; Itoh, H.; Yoshida, H. Reaction mechanism of aromatic ring hydroxylation by water over platinum-loaded titanium oxide photocatalyst. *J. Phys. Chem. C* **2012**, *116*, 25376–25387. [CrossRef]
20. AlSalka, Y.; Al-Madanat, O.; Curti, M.; Hakki, A.; Bahnemann, D.W. Photocatalytic H_2 evolution from oxalic acid: Effect of cocatalysts and carbon dioxide radical anion on the surface charge transfer mechanisms. *ACS Appl. Energy Mater.* **2020**, *3*, 6678–6691. [CrossRef]
21. Kandiel, T.A.; Feldhoff, A.; Robben, L.; Dillert, R.; Bahnemann, D.W. Tailored titanium dioxide nanomaterials: Anatase nanoparticles and brookite nanorods as highly active photocatalysts. *Chem. Mater.* **2010**, *22*, 2050–2060. [CrossRef]
22. Abdulrazzak, F.H.; Hussein, F.H.; Alkaim, A.F.; Ivanova, I.; Emeline, A.V.; Bahnemann, D.W. Sonochemical/hydration-dehydration synthesis of Pt-TiO_2 NPs/decorated carbon nanotubes with enhanced photocatalytic hydrogen production activity. *Photochem. Photobiol. Sci.* **2016**, *15*, 1347–1357. [CrossRef] [PubMed]
23. Colon, G.; Hidalgo, M.C.; Navio, J.A. Photocatalytic deactivation of commercial TiO_2 samples during simultaneous photoreduction of Cr(VI) and photooxidation of salicylic acid. *J. Photochem. Photobiol. A* **2001**, *138*, 79–85. [CrossRef]
24. Alonso-Tellez, A.; Masson, R.; Robert, D.; Keller, N.; Keller, V. Comparison of Hombikat UV100 and P25 TiO_2 performance in gas-phase photocatalytic oxidation reactions. *J. Photochem. Photobiol. A* **2012**, *250*, 58–65. [CrossRef]

25. Abellan, M.N.; Dillert, R.; Gimenez, J.; Bahnemann, D. Evaluation of two types of TiO_2-based catalysts by photodegradation of DMSO in aqueous suspension. *J. Photochem. Photobiol. A* **2009**, *202*, 164–171. [CrossRef]
26. AlSalka, Y.; Hakki, A.; Schneider, J.; Bahnemann, D.W. Co-catalyst-free photocatalytic hydrogen evolution on TiO_2: Synthesis of optimized photocatalyst through statistical material science. *Appl. Catal. B-Environ.* **2018**, *238*, 422–433. [CrossRef]
27. Chen, Y.; Wang, Y.; Li, W.; Yang, Q.; Hou, Q.; Wei, L.; Liu, L.; Huang, F.; Ju, M. Enhancement of photocatalytic performance with the use of noble-metal-decorated TiO_2 nanocrystals as highly active catalysts for aerobic oxidation under visible-light irradiation. *Appl. Catal. B-Environ.* **2017**, *210*, 352–367. [CrossRef]
28. Diebold, U. The surface science of titanium dioxide. *Surf. Sci. Rep.* **2003**, *48*, 53–229. [CrossRef]
29. Kowalska, E.; Remita, H.; Colbeau-Justin, C.; Hupka, J.; Belloni, J. Modification of titanium dioxide with platinum ions and clusters: Application in photocatalysis. *J. Phys. Chem. C* **2008**, *112*, 1124–1131. [CrossRef]
30. Kozlova, E.A.; Lyubina, T.P.; Nasalevich, M.A.; Vorontsov, A.V.; Miller, A.V.; Kaichev, V.V.; Parmon, V.N. Influence of the method of platinum deposition on activity and stability of Pt/TiO_2 photocatalysts in the photocatalytic oxidation of dimethyl methylphosphonate. *Catal. Commun.* **2011**, *12*, 597–601. [CrossRef]
31. Kandiel, T.A.; Dillert, R.; Robben, L.; Bahnemann, D.W. Photonic efficiency and mechanism of photocatalytic molecular hydrogen production over platinized titanium dioxide from aqueous methanol solutions. *Catal. Today* **2011**, *161*, 196–201. [CrossRef]
32. Abdel-Azim, S.M.; Aboul-Gheit, A.K.; Ahmed, S.M.; El-Desouki, D.S.; Abdel-Mottaleb, M.S.A. Preparation and application of mesoporous nanotitania photocatalysts using different templates and PH media. *Int. J. Photoenergy* **2014**, *2014*, 1–11. [CrossRef]
33. Wenderich, K.; Mul, G. Methods, mechanism, and applications of photodeposition in photocatalysis: A review. *Chem. Rev.* **2016**, *116*, 14587–14619. [CrossRef]
34. Al-Azri, Z.H.N.; AlOufi, M.; Chan, A.; Waterhouse, G.I.N.; Idriss, H. Metal particle size Effects on the photocatalytic hydrogen ion reduction. *ACS Catal.* **2019**, *9*, 3946–3958. [CrossRef]
35. Li, H.; Yu, H.; Sun, L.; Zhai, J.; Han, X. A self-assembled 3D Pt/TiO_2 architecture for high-performance photocatalytic hydrogen production. *Nanoscale* **2015**, *7*, 1610–1615. [CrossRef]
36. Xing, J.; Li, Y.H.; Jiang, H.B.; Wang, Y.; Yang, H.G. The size and valence state effect of Pt on photocatalytic H_2 evolution over platinized TiO_2 photocatalyst. *Int. J. Hydrog. Energy* **2014**, *39*, 1237–1242. [CrossRef]
37. Wang, D.; Liu, Z.P.; Yang, W.M. Revealing the size effect of platinum cocatalyst for photocatalytic hydrogen evolution on TiO_2 support: A DFT study. *ACS Catal.* **2018**, *8*, 7270–7278. [CrossRef]
38. Chen, H.R.; Li, P.; Umezawa, N.; Abe, H.; Ye, J.H.; Shiraishi, K.; Ohta, A.; Miyazaki, S. Bonding and electron energy-level alignment at metal/TiO_2 interfaces: A density functional theory study. *J. Phys. Chem. C* **2016**, *120*, 5549–5556. [CrossRef]
39. Su, R.; Bechstein, R.; So, L.; Vang, R.T.; Sillassen, M.; Esbjornsson, B.; Palmqvist, A.; Besenbacher, F. How the anatase-to-rutile ratio influences the photoreactivity of TiO_2. *J. Phys. Chem. C* **2011**, *115*, 24287–24292. [CrossRef]
40. Riegel, G.; Bolton, J.R. Photocatalytic efficiency variability in TiO_2 particles. *J. Phys. Chem.* **1995**, *99*, 4215–4224. [CrossRef]
41. Scanlon, D.O.; Dunnill, C.W.; Buckeridge, J.; Shevlin, S.A.; Logsdail, A.J.; Woodley, S.M.; Catlow, C.R.; Powell, M.J.; Palgrave, R.G.; Parkin, I.P.; et al. Band alignment of rutile and anatase TiO_2. *Nat. Mater.* **2013**, *12*, 798–801. [CrossRef]
42. Hurum, D.C.; Agrios, A.G.; Gray, K.A.; Rajh, T.; Thurnauer, M.C. Explaining the enhanced photocatalytic activity of Degussa P25 mixed-phase TiO_2 using EPR. *J. Phys. Chem. B* **2003**, *107*, 4545–4549. [CrossRef]
43. Dahl, M.; Liu, Y.; Yin, Y. Composite titanium dioxide nanomaterials. *Chem. Rev.* **2014**, *114*, 9853–9889. [CrossRef]
44. Hufschmidt, D.; Bahemann, D.; Testa, J.J.; Emilio, C.A.; Litter, M.I. Enhancement of the photocatalytic activity of various TiO_2 materials by platinisation. *J. Photochem. Photobiol. A* **2002**, *148*, 223–231. [CrossRef]
45. Sakthivel, S.; Shankar, M.V.; Palanichamy, M.; Arabindoo, B.; Bahnemann, D.W.; Murugesan, V. Enhancement of photocatalytic activity by metal deposition: Characterisation and photonic efficiency of Pt, Au and Pd deposited on TiO_2 catalyst. *Water Res.* **2004**, *38*, 3001–3008. [CrossRef]
46. Sun, B.; Vorontsov, A.V.; Smirniotis, P.G. Role of platinum deposited on TiO_2 in phenol photocatalytic oxidation. *Langmuir* **2003**, *19*, 3151–3156. [CrossRef]
47. Benz, D.; Felter, K.M.; Koser, J.; Thoming, J.; Mul, G.; Grozema, F.C.; Hintzen, H.T.; Kreutzer, M.T.; van Ommen, J.R. Assessing the role of Pt Clusters on TiO_2 (P25) on the photocatalytic degradation of acid blue 9 and rhodamine B. *J. Phys. Chem. C* **2020**, *124*, 8269–8278. [CrossRef]
48. Bamwenda, G.R.; Tsubota, S.; Nakamura, T.; Haruta, M. Photoassisted hydrogen production from a water-ethanol solution: A comparison of activities of Au-TiO_2 and Pt-TiO_2. *J. Photochem. Photobiol. A* **1995**, *89*, 177–189. [CrossRef]
49. Khan, M.R.; Chuan, T.W.; Yousuf, A.; Chowdhury, M.N.K.; Cheng, C.K. Schottky barrier and surface plasmonic resonance phenomena towards the photocatalytic reaction: Study of their mechanisms to enhance photocatalytic activity. *Catal. Sci. Technol.* **2015**, *5*, 2522–2531. [CrossRef]
50. Ola, O.; Maroto-Valer, M.M. Review of material design and reactor engineering on TiO_2 photocatalysis for CO_2 reduction. *J. Photochem. Photobiol. C.* **2015**, *24*, 16–42. [CrossRef]
51. Bui, T.D.; Kimura, A.; Ikeda, S.; Matsumura, M. Determination of oxygen sources for oxidation of benzene on TiO_2 photocatalysts in aqueous solutions containing molecular oxygen. *J. Am. Chem. Soc.* **2010**, *132*, 8453–8458. [CrossRef]
52. Pang, X.; Chen, C.; Ji, H.; Che, Y.; Ma, W.; Zhao, J. Unraveling the photocatalytic mechanisms on TiO_2 surfaces using the oxygen-18 isotopic label technique. *Molecules* **2014**, *19*, 16291–16311. [CrossRef]

53. Augugliaro, V.; Bellardita, M.; Loddo, V.; Palmisano, G.; Palmisano, L.; Yurdakal, S. Overview on oxidation mechanisms of organic compounds by TiO_2 in heterogeneous photocatalysis. *J. Photochem. Photobiol. C* **2012**, *13*, 224–245. [CrossRef]
54. Montoya, J.F.; Ivanova, I.; Dillert, R.; Bahnemann, D.W.; Salvador, P.; Peral, J. Catalytic role of surface oxygens in TiO_2 photooxidation reactions: Aqueous benzene photooxidation with $Ti^{18}O_2$ under anaerobic conditions. *J. Phys. Chem. Lett.* **2013**, *4*, 1415–1422. [CrossRef]
55. Bui, T.D.; Kimura, A.; Higashida, S.; Ikeda, S.; Mafsurnura, M. Two routes for mineralizing benzene by TiO_2-photocatalyzed reaction. *Appl. Catal. B-Environ.* **2011**, *107*, 119–127. [CrossRef]
56. Bui, T.D.; Kimura, A.; Ikeda, S.; Matsumura, M. Lowering of photocatalytic activity of TiO_2 particles during oxidative decomposition of benzene in aerated liquid. *Appl. Catal. B-Environ.* **2010**, *94*, 186–191. [CrossRef]
57. Panagiotopoulou, P.; Karamerou, E.E.; Kondarides, D.I. Kinetics and mechanism of glycerol photo-oxidation and photo-reforming reactions in aqueous TiO_2 and Pt/TiO_2 suspensions. *Catal. Today* **2013**, *209*, 91–98. [CrossRef]
58. Imizcoz, M.; Puga, A.V. Assessment of photocatalytic hydrogen production from biomass or wastewaters depending on the metal co-catalyst and Its deposition method on TiO_2. *Catalysts* **2019**, *9*, 584. [CrossRef]
59. Schneider, J.; Matsuoka, M.; Takeuchi, M.; Zhang, J.; Horiuchi, Y.; Anpo, M.; Bahnemann, D.W. Understanding TiO_2 photocatalysis: Mechanisms and materials. *Chem. Rev.* **2014**, *114*, 9919–9986. [CrossRef] [PubMed]
60. King, S.M.; Leaf, P.A.; Olson, A.C.; Ray, P.Z.; Tarr, M.A. Photolytic and photocatalytic degradation of surface oil from the Deepwater Horizon spill. *Chemosphere* **2014**, *95*, 415–422. [CrossRef] [PubMed]
61. Qourzal, S.; Assabbane, A.; Ait-Ichou, Y. Synthesis of TiO_2 via hydrolysis of titanium tetraisopropoxide and its photocatalytic activity on a suspended mixture with activated carbon in the degradation of 2-naphthol. *J. Photochem. Photobiol. A* **2004**, *163*, 317–321. [CrossRef]
62. Brahmia, O.; Richard, C. Photochemical transformation of 1-naphthol in aerated aqueous solution. *Photochem. Photobiol. Sci.* **2005**, *4*, 454–458. [CrossRef] [PubMed]
63. Weon, S.; Choi, W. TiO_2 nanotubes with open channels as deactivation-resistant photocatalyst for the degradation of volatile organic compounds. *Environ. Sci. Technol.* **2016**, *50*, 2556–2563. [CrossRef] [PubMed]
64. Theurich, J.; Bahnemann, D.W.; Vogel, R.; Ehamed, F.E.; Alhakimi, G.; Rajab, I. Photocatalytic degradation of naphthalene and anthracene: GC-MS analysis of the degradation pathway. *Res. Chem. Intermediat.* **1997**, *23*, 247–274. [CrossRef]
65. Mills, A.; Davies, R.H.; Worsley, D. Water-purification by semiconductor photocatalysis. *Chem. Soc. Rev.* **1993**, *22*, 417–425. [CrossRef]
66. Ajmal, A.; Majeed, I.; Malik, R.N.; Idriss, H.; Nadeem, M.A. Principles and mechanisms of photocatalytic dye degradation on TiO_2 based photocatalysts: A comparative overview. *RSC Adv.* **2014**, *4*, 37003–37026. [CrossRef]
67. Qourzal, S.; Barka, N.; Tamimi, M.; Assabbane, A.; Ait-Ichou, Y. Photodegradation of 2-naphthol in water by artificial light illumination using TiO_2 photocatalyst: Identification of intermediates and the reaction pathway. *Appl. Catal. A-Gen.* **2008**, *334*, 386–393. [CrossRef]
68. Denny, F.; Scott, J.; Chiang, K.; Teoh, W.Y.; Amal, R. Insight towards the role of platinum in the photocatalytic mineralisation of organic compounds. *J. Mol. Catal. A-Chem.* **2007**, *263*, 93–102. [CrossRef]
69. Hurum, D.C.; Agrios, A.G.; Crist, S.E.; Gray, K.A.; Rajh, T.; Thurnauer, M.C. Probing reaction mechanisms in mixed phase TiO_2 by EPR. *J. Electron. Spectrosc.* **2006**, *150*, 155–163. [CrossRef]
70. Howe, R.F.; Gratzel, M. EPR study of hydrated anatase under UV irradiation. *J. Phys. Chem.* **1987**, *91*, 3906–3909. [CrossRef]
71. Howe, R.F.; Gratzel, M. EPR observation of trapped electrons in colloidal titanium dioxide. *J. Phys. Chem.* **1985**, *89*, 4495–4499. [CrossRef]
72. Kumar, C.P.; Gopal, N.O.; Wang, T.C.; Wong, M.S.; Ke, S.C. EPR investigation of TiO_2 nanoparticles with temperature-dependent properties. *J. Phys. Chem. B* **2006**, *110*, 5223–5229. [CrossRef] [PubMed]
73. Shapovalov, V.; Stefanovich, E.V.; Truong, T.N. Nature of the excited states of the rutile TiO_2(110) surface with adsorbed water. *Surf. Sci.* **2002**, *498*, L103–L108. [CrossRef]
74. Nakaoka, Y.; Nosaka, Y. ESR Investigation into the effects of heat treatment and crystal structure on radicals produced over irradiated TiO_2 powder. *J. Photochem. Photobiol. A* **1997**, *110*, 299–305. [CrossRef]
75. Ke, S.C.; Wang, T.C.; Wong, M.S.; Gopal, N.O. Low temperature kinetics and energetics of the electron and hole traps in irradiated TiO_2 nanoparticles as revealed by EPR spectroscopy. *J. Phys. Chem. B* **2006**, *110*, 11628–11634. [CrossRef]
76. Connelly, K.; Wahab, A.K.; Idriss, H. Photoreaction of Au/TiO_2 for hydrogen production from renewables: A review on the synergistic effect between anatase and rutile phases of TiO_2. *Mater. Renew. Sustain. Energy* **2012**, *1*, 3. [CrossRef]
77. Arizavi, A.; Mirbagheri, N.S.; Hosseini, Z.; Chen, P.; Sabbaghi, S. Efficient removal of naphthalene from aqueous solutions using a nanoporous kaolin/Fe_3O_4 composite. *Int. J. Environ. Sci. Technol.* **2020**, *17*, 1991–2002. [CrossRef]
78. Nesterenko-Malkovskaya, A.; Kirzhner, F.; Zimmels, Y.; Armon, R. Eichhornia crassipes capability to remove naphthalene from wastewater in the absence of bacteria. *Chemosphere* **2012**, *87*, 1186–1191. [CrossRef]
79. Al-Madanat, O.; Curti, M.; Günnemann, C.; Alsalka, Y.; Dillert, R.; Bahnemann, D.W. TiO_2 photocatalysis: Impact of the platinum loading method on reductive and oxidative half-reactions. *Catal. Today* (under review).